Letter

Giant anisotropic band flattening in twisted Γ-valley semiconductor bilayers

Huan Wang [1,*] Zhaochen Liu,[1,*] Yadong Jiang [1] and Jing Wang [1,2,3,†]

[1]*State Key Laboratory of Surface Physics and Department of Physics, Fudan University, Shanghai 200433, China*
[2]*Institute for Nanoelectronic Devices and Quantum Computing, Fudan University, Shanghai 200433, China*
[3]*Zhangjiang Fudan International Innovation Center, Fudan University, Shanghai 201210, China*

(Received 6 September 2023; accepted 8 November 2023; published 28 November 2023)

We propose a general theory of anisotropic band flattening in moiré systems at the Γ valley. For a two-dimensional semiconductor with a rectangular unit cell of C_{2z} or mirror symmetries, we find that a larger effective mass anisotropy $\eta = m_y/m_x$ of the valence or conduction bands in the monolayer will have a stronger tendency to be further enhanced in its twisted bilayer. This gives rise to strong anisotropic band flattening and correlated physics in one dimension (1D) effectively. We predict twisted bilayer black phosphorus (tBBP) has giant anisotropic flattened moiré bands ($\eta \sim 10^4$) from *ab initio* calculations and the continuum model, where the low-energy physics is described by the weakly coupled array of 1D wires. We further calculate the phase diagram based on the sliding Luttinger liquid by including the screened Coulomb interactions in tBBP and find a large parameter space may host the non-Fermi liquid phase. We thus establish tBBP as a promising and experimentally accessible platform for exploring correlated physics in low dimensions.

DOI: 10.1103/PhysRevB.108.L201120

Introduction. Moiré materials with flat electronic bands provide an ideal platform for exploring strongly correlated physics in two dimensions (2D) [1–5]. A paradigm example is twisted bilayer graphene at the magic angle [6], which hosts flat bands and exhibits a variety of interacting phases including superconductors, correlated insulators, and Chern insulators [7–14]. Similar correlated phases have been observed in moiré systems of transition metal dichalcogenides [15–18] and multilayer graphene [19–21]. The correlated behaviors in moiré systems are associated with the quenched kinetic energy caused by the moiré pattern, so strong electron interaction could dominate.

An important correlated phase is the anisotropic non-Fermi liquid (non-FL), which is the Luttinger liquid (LL) model generalized to higher dimensions and could arise in 2D systems consisting of arrays of one-dimensional (1D) quantum wires [22–28]. Experimentally realizing these coupled wire arrays perfectly is challenging. Most of the previous efforts have been made in the context of quasi-1D organic conductors [29,30]. Recently, such anisotropic correlated phases may have been observed in twisted bilayer WTe_2 [31], which may host 1D flat bands [32] and exhibit LL behavior in a 2D crystal. The anisotropic band flattening occurs when low-energy physics is located on the Brillouin zone edge but not at the zone corner [33–35] and is guaranteed by symmetry. However, realistic 2D materials fulfilling such requirements are extremely rare, while large classes of 2D semiconductors have the valence band top or conduction band bottom occurring at the Γ valley, namely, the Brillouin zone center. This motivates us to study whether the 1D flat band could arise in a twisted bilayer of the Γ valley systems and further identify realistic platforms in which the LL phase and other exotic phases of matter may appear.

We develop the theory of anisotropic band flattening in a twisted bilayer of the Γ valley system. For a 2D crystal with a rectangular unit cell of C_{2z} or mirror symmetries, we find that a larger effective mass anisotropy of the valence or conduction bands in the monolayer will have a stronger tendency to be further enhanced in its twisted bilayer. Namely, the anisotropic band flattening occurs over most of the phase space if the monolayer has large effective mass anisotropy. We propose twisted bilayer black phosphorus (tBBP) as a concrete example with giant anisotropic flattened moiré bands, where the low-energy physics is described by the weakly coupled array of 1D wires from the real-space charge density calculations. We further calculate the finite temperature phase diagram based on the screened Coulomb interactions and propose tBBP as a promising and experimentally accessible platform for observing exotic non-FL behavior in 2D.

Model. We present band engineering by starting from the twisted bilayer with generic anisotropic band dispersions in each layer, where the low-energy physics is at Γ. The general theory for the anisotropic band flattening presented here is generic for any semiconductors with anisotropic electronic dispersions in the valence or conduction bands. For simplicity, we first assume that each layer is a nonmagnetic rectangular lattice with a minimal C_{2z} symmetry. We consider stacking of two identical layers taking the z axis as a normal direction. The top and bottom layers are rotated by small angles $+\varphi/2$ and $-\varphi/2$ around the z axis, respectively. Here, $\mathbf{a}_1$ and $\mathbf{a}_2$ are the Bravais unit vectors of a monolayer rectangular lattice. Then the twisted moiré pattern has the periodicity of $\mathbf{L}_1$ and $\mathbf{L}_2$ as $\mathbf{L}_i = -\hat{\mathbf{z}} \times \mathbf{a}_i/[2\sin(\varphi/2)]$. The generic effective model

*These two authors contributed equally to this work.
†Corresponding author: wjingphys@fudan.edu.cn

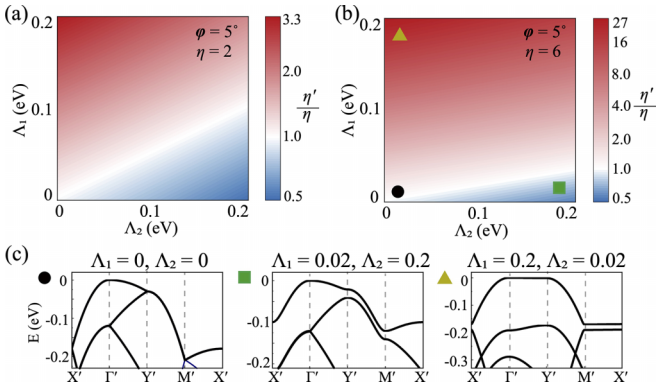

FIG. 1. The evolution of effective mass anisotropy η' of Γ valley under moiré pattern. (a) and (b) The ratio η'/η vs Λ_i for twist angle $\varphi = 5^\circ$ and monolayer effective mass anisotropy $\eta = 2$ and 6, respectively. (c) Typical moiré band structures indicated by the symbols in (b). The anisotropic band flattening occurs in the yellow triangle, and the topmost bands are twofold degenerate from $\Lambda_0 = 0$. $a_1 = 4.0$ Å, $a_2 = 3.9$ Å.

for electrons in such a moiré pattern is written as

$$\mathcal{H}_{\text{eff}} = \begin{bmatrix} H_t(-i\nabla) & \Lambda(\mathbf{r}) \\ \Lambda^\dagger(\mathbf{r}) & H_b(-i\nabla) \end{bmatrix}. \tag{1}$$

Here, $H_{t/b}$ are the kinetic energy in the top/bottom layer, which takes the general form as $H^\Gamma_{t/b}(\mathbf{k}) = k_x^2/2m_x + k_y^2/2m_y$, with the momentum $k_{x/y} \in (-\pi/a_{1/2}, \pi/a_{1/2}]$. The effective mass anisotropy is defined as $\eta \equiv m_y/m_x$. The moiré potential $\Lambda(\mathbf{r})$ is spatially periodic with the periodicity $\mathbf{L}_1$ and $\mathbf{L}_2$, which can be Fourier expanded by considering C_{2z} and time reversal $\mathcal{T}$ symmetries of the Γ valley as

$$\Lambda(\mathbf{r}) = \Lambda_0 + \sum_{n,i} \Lambda(\mathbf{g}_{n,i}) \cos(\mathbf{g}_{n,i} \cdot \mathbf{r}), \tag{2}$$

where $\mathbf{g}_{n,i}$ denote the moiré reciprocal lattice vectors to the nth moiré Brillouin zone (mBZ) and $\Lambda(\mathbf{g}_{n,i})$ is real.

Mass anisotropy under moiré pattern. By diagonalizing Eq. (1), we obtain the moiré band structure. The low-energy physics still occurs at Γ, and the effective Hamiltonian now becomes $H^{\text{moiré}}_\Gamma = k_x'^2/2m_x' + k_y'^2/2m_y'$, where $k'_{x/y} \in (-\pi/L_{2/1}, \pi/L_{2/1}]$. Then we can see how effective mass anisotropy $\eta' \equiv m_y'/m_x'$ evolves under moiré potential. For simplicity, we only consider $\mathbf{g}_{n,i}$ up to the first mBZ, namely, $n = 1$, and $\Lambda(\mathbf{g}_{1,i}) \equiv \Lambda_i$; we set $\Lambda_0 = 0$.

Figure 1 shows the effective mass anisotropy ratio η'/η as a function of Λ_i at twist angle $\varphi = 5^\circ$. In Fig. 1(a), we set monolayer $\eta = 2$, with $m_x = -0.1m_0$, $m_y = -0.2m_0$, and m_0 is the mass of free electron. In Fig. 1(b), $\eta = 6$, with $m_x = -0.1m_0$, $m_y = -0.6m_0$. In Figs. 1(a) and 1(b), the $\eta'/\eta = 1$ line is colored white, while red and blue regions denote the effective mass anisotropy is enhanced and suppressed under the moiré potential, respectively. If the monolayer system is isotropic $\eta = 1$, then $\eta'/\eta = 1$ is along the diagonal line $\Lambda_1 = \Lambda_2$ in phase space. Two conclusions can be drawn here. First, as the monolayer anisotropy η gets larger, the area of anisotropy enhanced part ($\eta/\eta > 1$) of the phase space in the twisted bilayer becomes bigger. This simply means the more anisotropic the monolayer system, the stronger the tendency to get larger anisotropy in its twisted system. Second, as η becomes larger, the effect of anisotropy enhancement gets better even when Λ_i is the same. We can see the maximum of $(\eta'/\eta)_{\max} = 3.3$ in Fig. 1(a), while in Fig. 1(b), it becomes $(\eta'/\eta)_{\max} = 27$, even though η of the monolayer is of the same order of magnitude.

The above mass anisotropy behaviors can be understood from the band-folding picture perturbatively. When $\Lambda(\mathbf{r}) = 0$, the folded band structure is shown in Fig. 1(c), where the topmost valence bands are degenerate at Brillouin zone boundaries X′, Y′, and M′. When $\Lambda(\mathbf{r}) \neq 0$, in the small angle limit, $H_{t/b}$ scales as $1/|\mathbf{L}_i|^2$ and becomes less important, and $\Lambda(\mathbf{r})$ dominates. Then by treating $H_{t/b}$ as perturbations, we can diagonalize $\mathcal{H}_{\text{eff}}$ in which $\Lambda(\mathbf{r})$ is diagonalized:

$$\widetilde{\mathcal{H}}_{\text{eff}} = \begin{bmatrix} H_t(-i\nabla) + |\Lambda(\mathbf{r})| & 0 \\ 0 & H_b(-i\nabla) - |\Lambda(\mathbf{r})| \end{bmatrix}. \tag{3}$$

We can see that $|\Lambda(\mathbf{r})|$ plays a role in the potential energy. Here, $|\Lambda_1|$ and $|\Lambda_2|$ are the potential heights along the $\mathbf{a}_2$ and $\mathbf{a}_1$ axes, respectively, which open the gap at Y′ and X′. Intuitively, the potential tends to confine the electrons with large effective mass and small kinetic energy more effectively, while the electrons with small effective mass and large kinetic energy tend to move freely in such a potential. The moiré bandwidths along Γ′-Y′ and Γ′-X′ are approximately $\pi^2/2|m_y|L_1^2 - |\Lambda_1|/2$ and $\pi^2/2|m_x|L_2^2 - |\Lambda_2|/2$, respectively. Thus, the mass anisotropy ratio becomes

$$\frac{\eta'}{\eta} \approx \frac{\pi^2 - |m_x\Lambda_2|L_2^2}{\pi^2 - |m_y\Lambda_1|L_1^2} \equiv \frac{1 - \Lambda_2/2W_1}{1 - \Lambda_1/2W_2}, \tag{4}$$

where $W_{1,2} \equiv \pi^2/2|m_{x,y}|L_{2,1}^2$ is the bandwidth along Γ′-X′, Γ′-Y′ of the mBZ. It is not easy to see the relation between η'/η and η directly. To further simplify Eq. (4), we set $L_1 \sim L_2 \sim L$ and $\Lambda_1 \sim \Lambda_2 \sim \lambda$, then

$$\frac{\eta'}{\eta} \approx \frac{W - \lambda}{W - \lambda\eta}, \tag{5}$$

with $W \equiv \pi^2/m_xL^2$. Both the numerator and denominator in Eq. (5) are positive under the perturbative treatment; thus, when $\eta > 1$, $\eta'/\eta > 1$; and when $\eta \gg 1$, we have $(W - \lambda\eta) \to 0^+$, then $\eta'/\eta \gg 1$. So the guiding principle to have a stronger anisotropic band flattening is to start with a larger anisotropy monolayer system.

Black phosphorus. To demonstrate the feasibility of our theory, we search for realistic materials. A paradigm example of 2D materials with strong anisotropic electronic dispersion is black phosphorus [36,37]. The monolayer black phosphorus has a rectangular lattice with the space group *Pmna*1′ (No. 53). The symmetry operations include $\{C_{2z}|\frac{1}{2}, \frac{1}{2}\}$, $\{C_{2x}|\frac{1}{2}, \frac{1}{2}\}$, M_y, and $\mathcal{T}$. As shown in Fig. 2(a), each primitive cell includes four phosphorus atoms. The low-energy physics is around Γ and is contributed from p_z orbitals, where we find strong mass anisotropy $m_x = -0.2m_0$ and $m_y = -1.8m_0$ by fitting with *ab initio* calculations in Fig. 1(a), namely, $\eta = 9$.

Then we study the moiré band structure of tBBP. The moiré superlattice is shown in Fig. 2(b). Quite different from the moiré superlattice of tungsten in twisted WTe_2 [31], there are no clear 1D stripes here. Since the translational symmetry is broken by the moiré pattern, the interlayer coupling $\Lambda(\mathbf{r})$ only respects M_y and $\mathcal{T}$ symmetries. By expanding to the first

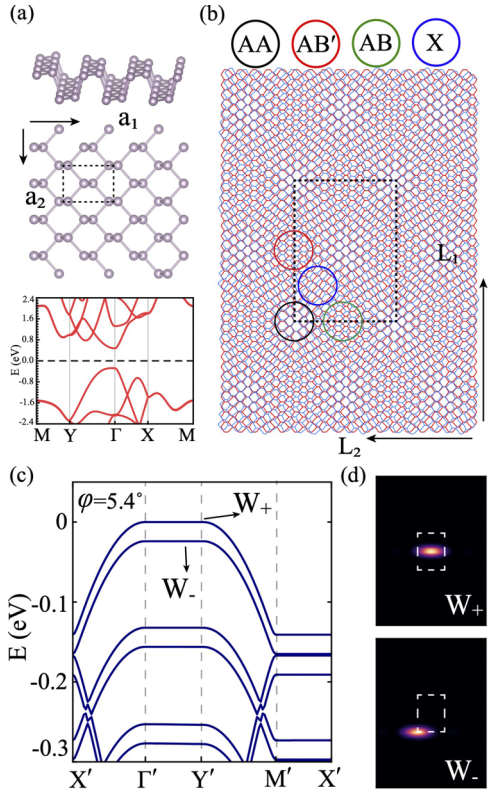

FIG. 2. Small-angle twisted bilayer black phosphorus (tBBP) moiré lattice and electronic properties. (a) Crystal structure and band structure of monolayer black phosphorus; the dashed rectangle indicates the unit cell. (b) Moiré superlattice formed on tBBP, where colored circles label several high-symmetry local stacking structures, with in-plane relative shift $\tau_{AA} = \mathbf{0}$, $\tau_{AB'} = \mathbf{a}_1/2$, $\tau_{AB} = \mathbf{a}_2/2$, and $\tau_X = \mathbf{a}_1/4 + \mathbf{a}_2/4$. (c) The moiré band structure from continuum model, and (d) the Wannier functions of the two topmost bands, where the white rectangle labels the size of a moiré unit cell.

mBZ, $\Lambda(\mathbf{r})$ can be expressed as

$$\Lambda_{BP}(\mathbf{r}) = \Lambda_0 + \sum_{i=1}^{4} \Lambda(\mathbf{g}_{1,i}) \exp(i\mathbf{g}_{1,i} \cdot \mathbf{r}),$$
$$\Lambda(\mathbf{g}_{1,1}) = \Lambda^*(\mathbf{g}_{1,3}) = \lambda_1 + i\lambda_3,$$
$$\Lambda(\mathbf{g}_{1,2}) = \Lambda(\mathbf{g}_{1,4}) = \lambda_2. \quad (6)$$

Here, $\mathbf{g}_{1,1/2}$ is the moiré reciprocal lattice vector to the first mBZ, $\mathbf{g}_{1,3/4} = -\mathbf{g}_{1,1/2}$. Also, Λ_0 and λ_j $(j = 1, 2, 3)$ are real parameters, which can be obtained by fitting the band structures from *ab initio* calculations with untwisted but shifted configurations such as AA, AB′, AB, and X shown in Fig. 2(b) [38,39]. We find $\Lambda_0 = 12$ meV, $\lambda_1 = 137$ meV, $\lambda_2 = 13$ meV, and $\lambda_3 = -10$ meV.

The band structure of tBBP with $\varphi = 5.4^\circ$ is shown in Fig. 2(c), where the two topmost valence bands have a giant anisotropic band flattening of $\eta' \approx 2 \times 10^4$, as shown in Fig. 4(c). These two bands are only dispersive along the Γ′-Y′ (or X′-M′) direction and dispersionless along the perpendicular Γ′-X′ (or Y′-M′) direction. A similar band structure from *ab initio* calculations is obtained in the Supplemental Material [39–41]. In Fig. 2(c), the two topmost valence bands are from the trapping at two local maximum

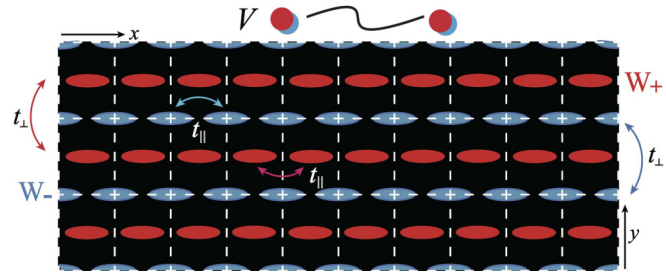

FIG. 3. Schematics of array of parallel weakly coupled one-dimensional (1D) wires. White dashed rectangle denotes the moiré unit cell, red ellipse is the layer bonding state W_+ at the center of unit cell, blue ellipse is the layer antibonding state W_- at the corner of unit cell. $t_\perp$ and $t_\parallel$ are the interwire and intrawire hopping, respectively. V is the long-range Coulomb interaction.

points of moiré potential $|\Lambda_{BP}(\mathbf{r})|$, which are located at the corner and middle of the unit cell, respectively. The potentials at these two points are different due to finite Λ_0, thus leading to splitting of the two topmost bands compared with degenerate bands with $\Lambda_0 = 0$ in Fig. 1(c). We further construct the maximally localized Wannier functions of these two bands [42]. As shown in Fig. 2(d), we find the Wannier state of top band W_+ is localized at the center of the moiré unit cell and represents a layer bonding state for $\Lambda_{BP}(\mathbf{r})$ is positive, while the Wannier state of the second topmost band W_- is localized at the corner of moiré unit cell and is a layer antibonding state for negative $\Lambda_{BP}(\mathbf{r})$. Both of the Wannier states are highly anisotropic in real space.

Weakly coupled 1D wires array. With giant anisotropic flatten moiré bands, tBBP now is described by the array of weakly coupled 1D wires illustrated in Fig. 3, which can expand the LL physics to 2D. Here, we study the effect of the Coulomb interaction in this system. The lattice Hamiltonian is constructed by projecting the single-particle model and Coulomb interaction onto the above two maximally localized Wannier states. Since these Wannier states are well localized and separated from each other, we only keep the on-site Hubbard term and long-ranged density-density interaction, and other interactions such as exchange, paired hopping, and correlated hopping have been neglected. The bosonized form of the 1D fermion operator is $\psi_{s,r,j}(x) = (\zeta_{r,s,j}/\sqrt{2\pi\varepsilon}) \exp(irk_F x) \exp[-i(r\phi_{s,j} - \theta_{s,j})]$, where ε is related to the intrachain cutoff with the dimension of length, $r = \pm$ stands for the right- and left-moving electrons, $s = \uparrow, \downarrow$ is the spin index, j denotes the wire number, $\zeta_{r,s,j}$ is the Kelvin factor, $\phi_{s,j}$ is the density variable, and $\theta_{s,j}$ is the conjugate phase variable [43,44]. The boson operators for charge and spin excitations are given by $\phi_{\rho,j} = (\phi_{\uparrow,j} + \phi_{\downarrow,j})/\sqrt{2}$ and $\phi_{\sigma,j} = (\phi_{\uparrow,j} - \phi_{\downarrow,j})/\sqrt{2}$, respectively, and a similar relation for the dual θ field. For the array of 1D wires, we can write an effective Hamiltonian as

$$\mathcal{H}_{1d} = \frac{1}{2\pi\Omega a_y} \sum_q \sum_{\beta=\rho,\sigma} u_\beta q_x^2 \Big[K_\beta(q)\theta_{\beta,q}\theta_{\beta,-q} + \frac{1}{K_\beta(q)}\phi_{\beta,q}\phi_{\beta,-q} \Big] + \sum_j \int dx \frac{2U a_x}{(2\pi\varepsilon)^2} \cos\sqrt{8}\phi_{j,\sigma}, \quad (7)$$

where a_x and a_y are intrachain and interchain lattice constants, respectively. Here, Ω is the system area, U is the Hubbard interaction strength. We assume the noncommensurate filling; thus, the Umklapp process in the charge sector of Hubbard term cannot exist. Also, we only keep the forward scattering in the long-range density-density interaction [44]. The Luttinger parameter and velocity are $u_\rho K_\rho = v_F, u_\rho/K_\rho = v_F + Ua_x/\pi + 2V(q)/\pi a_y$ and $u_\sigma K_\sigma = v_F, u_\sigma/K_\sigma = v_F - Ua_x/\pi$. Here, $V(q)$ is the Fourier-transformed Coulomb interaction. Here, we consider the single-gate-screened Coulomb interaction with $V(q) = [1 - \exp(-2d_s q)]e^2/2\epsilon\epsilon_0 q$, where d_s is the distance between the sample and gate, we set $d_s = 50$ nm, and ϵ is dielectric constant of the substrate. The spin sector with the bare Luttinger parameter in the attractive interaction regime (i.e., $K_\sigma > 1$) flows to the gapless phase with $K_\sigma = 1$ under the renormalization group (RG), which is imposed by spin SU(2) symmetry. Thus, the last term in $\mathcal{H}_{1d}$ vanishes [44].

Now we can see $\mathcal{H}_{1d}$ with the remaining first term is just the generic form of sliding LL. The instabilities of this model under various interaction couplings have been studied perviously [23–27]. The most relevant interactions are interchain electron tunneling (ET), charge-density wave (CDW), and superconducting couplings (SCs), which are expressed as

$$\mathcal{H}_{\mathrm{ET},n} \propto \sum_{s,r,j} \int dx \psi^\dagger_{s,r,j}\psi_{s,r,j+n} + \mathrm{H.c.} \propto \sum_j \int dx \sum_{s=\uparrow,\downarrow} \cos(\phi_{s,j} - \phi_{s,j+n}) \cos(\theta_{s,j} - \theta_{s,j+n}), \tag{8}$$

$$\mathcal{H}_{\mathrm{SC},n} \propto \sum_j \int dx (\psi^\dagger_{R,\uparrow,j}\psi^\dagger_{L,\downarrow,j} + \psi^\dagger_{R,\downarrow,j}\psi^\dagger_{L,\uparrow,j})(\psi_{R,\uparrow,j+n}\psi_{L,\downarrow,j+n} + \psi_{R,\downarrow,j+n}\psi_{L,\uparrow,j+n}) + \mathrm{H.c.}$$

$$\propto \sum_j \int dx \cos\sqrt{2}(\theta_{\rho,j} - \theta_{\rho,j+n}) \cos\sqrt{2}\phi^\sigma_j \cos\sqrt{2}\phi^\sigma_{j+n}, \tag{9}$$

$$\mathcal{H}_{\mathrm{CDW},n} \propto \sum_j \int dx (\psi^\dagger_{R,\uparrow,j}\psi_{L,\uparrow,j} + \psi^\dagger_{R,\downarrow,j}\psi_{L,\downarrow,j})\left(\psi^\dagger_{L,\uparrow,j+n}\psi_{R,\uparrow,j+n} + \psi^\dagger_{L,\downarrow,j+n}\psi_{R,\downarrow,j+n}\right) + \mathrm{H.c.}$$

$$\propto \sum_j \int dx \cos\sqrt{2}(\phi_{\rho,j} - \phi_{\rho,j+n}) \cos\sqrt{2}\phi^\sigma_j \cos\sqrt{2}\phi^\sigma_{j+n}. \tag{10}$$

Here, $\mathcal{H}_{\alpha,n}$ (α = ET, SC, CDW) describe the coupling between chains separated by a distance of na_y. After projecting the Coulomb interaction $V(q)$ along the chain by $V(q_x = 0, q_y)$, we can obtain the scaling dimension $\Delta_{\alpha,n}$ for the coupling strength $J_{\alpha,n}$ of $H_{\alpha,n}$ as

$$\Delta_{\mathrm{CDW},n} = \int_{-\pi}^{\pi} \frac{dq_y}{2\pi}[1 - \cos(nq_y)]K_\rho(q_y) + 1,$$

$$\Delta_{\mathrm{SC},n} = \int_{-\pi}^{\pi} \frac{dq_y}{2\pi}[1 - \cos(nq_y)]K^{-1}_\rho(q_y) + 1,$$

$$\Delta_{\mathrm{ET},n} = \frac{1}{4}(\Delta_{\mathrm{SC},n} + \Delta_{\mathrm{CDW},n}). \tag{11}$$

Phase diagram and sliding LL. The screened Coulomb interaction decays rapidly in real space when the distance exceeds the screening length. Thus, it is legitimate to consider only the nearest neighbor ($n = 1$) coupling for CDW and SC couplings, while the leading order for ET is $n = 2$ because the tunneling between W_+ and W_- is exactly zero. The subscript n is now omitted. By varying the dielectric constant ϵ and twisting angle φ, we find the ET is the most relevant ($\Delta_{\mathrm{ET}} \approx 1.1$), and the CDW coupling is subdominant ($\Delta_{\mathrm{CDW}} \approx 1.7$), while the superconductivity is always irrelevant ($\Delta_{\mathrm{SC}} > 2$) [see Fig. 4(b)]. Therefore, we expect in the array of 1D wires a crossover from non-FL (namely, sliding LL) behavior to FL or CDW as the temperature is lowered, as shown in Fig. 4(d).

The finite-temperature phase diagram in tBBP where the crossover takes place is calculated in Fig. 4(a). The interactions renormalize the coupling strength, and upon rescaling the RG equation for J_α at tree level, we obtain $dJ_\alpha/dl = J_\alpha(2 - \Delta_\alpha)$. Here, $J_{\mathrm{ET}} = t_\perp$ and $J_{\mathrm{CDW}} \approx e^2/4\pi\epsilon\epsilon_0 a_y$. We determine the crossover scale by the energy at which the renormalized coupling strength is of order one $J_\alpha/W \sim 1$, where $W = 4t_\parallel$ is the order of the intrachain bandwidth. Thus,

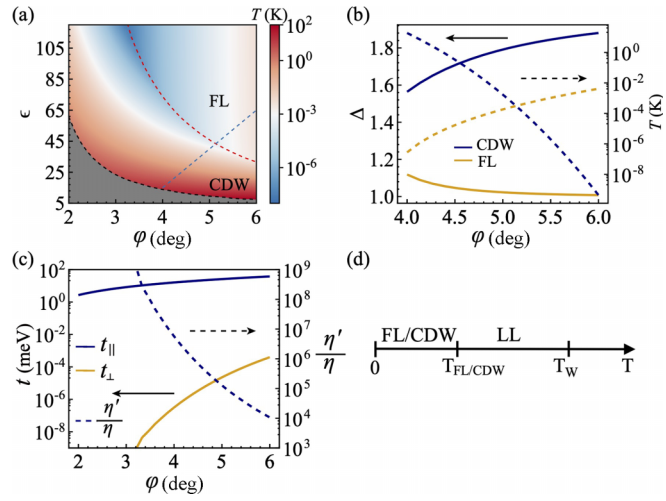

FIG. 4. (a) Finite-temperature phase diagram vs dielectric constant ϵ and twist angle φ in twisted bilayer black phosphorus (tBBP). Color shows the transition temperature of the corresponding phase. For the shaded region, the Hubbard interaction is larger than the bandwidth, which is inaccessible by the bosonization approach. (b) The scaling dimension (solid lines) and transition temperature (dashed lines) of charge-density wave (CDW) and Fermi liquid (FL) states along the blue dashed line in (a). The single-particle tunneling is most relevant. (c) $t_\parallel$, $t_\perp$, and η'/η vs φ in tBBP. (d) Schematic of dimensional crossover from sliding Luttinger liquid (LL) to CDW/FL.

$T_\alpha \sim W(J_\alpha/W)^{1/(2-\Delta_\alpha)}$ [30,44]. Since Δ_α is always >1 for an interacting system, we see that the temperature scale at which the crossover takes place is always smaller than the noninteracting case $T_\alpha \sim J_\alpha$. As shown in Fig. 4(a), although interchain single particle tunneling is the most relevant, there is still quite a region in the phase diagram where the transition temperature of the CDW phase is larger than that of a FL, caused by interchain ET. Meanwhile, the system very unlikely enters a FL state in the experimentally accessible low temperature, as shown in Fig. 4(b). Moreover, the energy scale of the intrachain bandwidth T_W in Fig. 4(c) ranges from 90 K ($\varphi = 2^\circ$) to 1700 K ($\varphi = 6^\circ$). Therefore, we expect the LL behavior can be observed over a wide temperature range ($T_{CDW/FL} < T < T_W$) in tBBP. In the shaded region in Fig. 4(a), the on-site Hubbard U is much larger than the bandwidth (thus, $K_\sigma^2 < 0$), which invalidates the bosonization approach, and the system is considered as the Hubbard model, and this is beyond the current scope of this letter.

Summary. In summary, we propose the guiding principle for a stronger anisotropic band flattening in the Γ valley moiré system is to start with a larger anisotropy monolayer system, such as but not limited to the rectangular lattice with C_{2z} or mirror symmetries. We predict tBBP as a paradigm example with giant anisotropic flattened moiré bands, which provides a highly tunable platform for studying the weakly coupled 2D array of 1D electronic structures. The interchain hopping with several orders of magnitude smaller compared with intrachain hopping in tBBP gives rise to a wide temperature range to observe the LL behavior in 2D. The twisted multilayer black phosphorus is also expected to host anisotropic flattened 1D bands. The rich choice of Γ valley 2D semiconductors (for example, black arsenic [45]) provides great opportunities for studying many correlated and topological quantum phases [23–26,46–50].

Acknowledgments. We acknowledge helpful discussions with Biao Lian and Yuanbo Zhang. This letter is supported by the National Key Research Program of China under Grant No. 2019YFA0308404, the Natural Science Foundation of China through Grant No. 12174066, the Innovation Program for Quantum Science and Technology through Grant No. 2021ZD0302600, Science and Technology Commission of Shanghai Municipality under Grants No. 20JC1415900 and No. 23JC1400600, Shanghai Municipal Science and Technology Major Project under Grant No. 2019SHZDZX01.

[1] E. Y. Andrei and A. H. MacDonald, Graphene bilayers with a twist, Nat. Mater. **19**, 1265 (2020).
[2] L. Balents, C. R. Dean, D. K. Efetov, and A. F. Young, Superconductivity and strong correlations in moiré flat bands, Nat. Phys. **16**, 725 (2020).
[3] S. Carr, S. Fang, and E. Kaxiras, Electronic-structure methods for twisted moiré layers, Nat. Rev. Mater. **5**, 748 (2020).
[4] D. M. Kennes, M. Claassen, L. Xian, A. Georges, A. J. Millis, J. Hone, C. R. Dean, D. N. Basov, A. N. Pasupathy, and A. Rubio, Moiré heterostructures as a condensed-matter quantum simulator, Nat. Phys. **17**, 155 (2021).
[5] E. Y. Andrei, D. K. Efetov, P. Jarillo-Herrero, A. H. MacDonald, K. F. Mak, T. Senthil, E. Tutuc, A. Yazdani, and A. F. Young, The marvels of moiré materials, Nat. Rev. Mater. **6**, 201 (2021).
[6] R. Bistritzer and A. H. MacDonald, Moiré bands in twisted double-layer graphene, Proc. Natl. Acad. Sci. USA **108**, 12233 (2011).
[7] Y. Cao, V. Fatemi, S. Fang, K. Watanabe, T. Taniguchi, E. Kaxiras, and P. Jarillo-Herrero, Unconventional superconductivity in magic-angle graphene superlattices, Nature (London) **556**, 43 (2018).
[8] Y. Cao, V. Fatemi, A. Demir, S. Fang, S. L. Tomarken, J. Y. Luo, J. D. Sanchez-Yamagishi, K. Watanabe, T. Taniguchi, E. Kaxiras *et al.*, Correlated insulator behaviour at half-filling in magic-angle graphene superlattices, Nature (London) **556**, 80 (2018).
[9] M. Yankowitz, S. Chen, H. Polshyn, Y. Zhang, K. Watanabe, T. Taniguchi, D. Graf, A. F. Young, and C. R. Dean, Tuning superconductivity in twisted bilayer graphene, Science **363**, 1059 (2019).
[10] A. L. Sharpe, E. J. Fox, A. W. Barnard, J. Finney, K. Watanabe, T. Taniguchi, M. A. Kastner, and D. Goldhaber-Gordon, Emergent ferromagnetism near three-quarters filling in twisted bilayer graphene, Science **365**, 605 (2019).
[11] X. Lu, P. Stepanov, W. Yang, M. Xie, M. A. Aamir, I. Das, C. Urgell, K. Watanabe, T. Taniguchi, G. Zhang *et al.*, Superconductors, orbital magnets and correlated states in magic-angle bilayer graphene, Nature (London) **574**, 653 (2019).
[12] M. Serlin, C. L. Tschirhart, H. Polshyn, Y. Zhang, J. Zhu, K. Watanabe, T. Taniguchi, L. Balents, and A. F. Young, Intrinsic quantized anomalous Hall effect in a moiré heterostructure, Science **367**, 900 (2020).
[13] K. P. Nuckolls, M. Oh, D. Wong, B. Lian, K. Watanabe, T. Taniguchi, B. A. Bernevig, and A. Yazdani, Strongly correlated Chern insulators in magic-angle twisted bilayer graphene, Nature (London) **588**, 610 (2020).
[14] Y. Xie, A. T. Pierce, J. M. Park, D. E. Parker, E. Khalaf, P. Ledwith, Y. Cao, S. H. Lee, S. Chen, P. R. Forrester *et al.*, Fractional Chern insulators in magic-angle twisted bilayer graphene, Nature (London) **600**, 439 (2021).
[15] Y. Xu, S. Liu, D. A. Rhodes, K. Watanabe, T. Taniguchi, J. Hone, V. Elser, K. F. Mak, and J. Shan, Correlated insulating states at fractional fillings of Moiré superlattices, Nature (London) **587**, 214 (2020).
[16] B. A. Foutty, C. R. Kometter, T. Devakul, A. P. Reddy, K. Watanabe, T. Taniguchi, L. Fu, and B. E. Feldman, Mapping twist-tuned multi-band topology in bilayer WSe_2, arXiv:2304.09808.
[17] J. Cai, E. Anderson, C. Wang, X. Zhang, X. Liu, W. Holtzmann, Y. Zhang, F. Fan, T. Taniguchi, K. Watanabe *et al.*, Signatures of fractional quantum anomalous Hall states in twisted $MoTe_2$, Nature (London) **622**, 63 (2023).
[18] Y. Zeng, Z. Xia, K. Kang, J. Zhu, P. Knüppel, C. Vaswani, K. Watanabe, T. Taniguchi, K. F. Mak, and J. Shan, Thermodynamic evidence of fractional Chern insulator in Moiré $MoTe_2$, Nature (London) **622**, 69 (2023).
[19] G. Chen, A. L. Sharpe, P. Gallagher, I. T. Rosen, E. J. Fox, L. Jiang, B. Lyu, H. Li, K. Watanabe, T. Taniguchi *et al.*,

Signatures of tunable superconductivity in a trilayer graphene Moiré superlattice, Nature (London) **572**, 215 (2019).

[20] Z. Hao, A. M. Zimmerman, P. Ledwith, E. Khalaf, D. H. Najafabadi, K. Watanabe, T. Taniguchi, A. Vishwanath, and P. Kim, Electric field-tunable superconductivity in alternating-twist magic-angle trilayer graphene, Science **371**, 1133 (2021).

[21] J. M. Park, Y. Cao, K. Watanabe, T. Taniguchi, and P. Jarillo-Herrero, Tunable strongly coupled superconductivity in magic-angle twisted trilayer graphene, Nature (London) **590**, 249 (2021).

[22] X. G. Wen, Metallic non-Fermi-liquid fixed point in two and higher dimensions, Phys. Rev. B **42**, 6623 (1990).

[23] V. J. Emery, E. Fradkin, S. A. Kivelson, and T. C. Lubensky, Quantum theory of the smectic metal state in stripe phases, Phys. Rev. Lett. **85**, 2160 (2000).

[24] A. Vishwanath and D. Carpentier, Two-dimensional anisotropic non-Fermi-liquid phase of coupled Luttinger liquids, Phys. Rev. Lett. **86**, 676 (2001).

[25] R. Mukhopadhyay, C. L. Kane, and T. C. Lubensky, Sliding Luttinger liquid phases, Phys. Rev. B **64**, 045120 (2001).

[26] S. L. Sondhi and K. Yang, Sliding phases via magnetic fields, Phys. Rev. B **63**, 054430 (2001).

[27] S. Sur and K. Yang, Coulomb interaction driven instabilities of sliding Luttinger liquids, Phys. Rev. B **96**, 075131 (2017).

[28] X. Song, T. Zhang, H. Yang, H. Ji, J. Sun, L. Liu, Y. Wang, and H. Gao, Intriguing one-dimensional electronic behavior in emerging two-dimensional materials, Nano Res. **14**, 3810 (2021).

[29] D. Jérome, Organic superconductors: From $(TMTSF)_2PF_6$ to fullerenes, in *Organic Conductors: Fundamentals and Applications*, edited by J.-P. Farges (CRC Press, Boca Raton, 1994), Chap. 10, p. 405.

[30] A. Georges, T. Giamarchi, and N. Sandler, Interchain conductivity of coupled Luttinger liquids and organic conductors, Phys. Rev. B **61**, 16393 (2000).

[31] P. Wang, G. Yu, Y. H. Kwan, Y. Jia, S. Lei, S. Klemenz, F. A. Cevallos, R. Singha, T. Devakul, K. Watanabe *et al.*, One-dimensional Luttinger liquids in a two-dimensional moiré lattice, Nature (London) **605**, 57 (2022).

[32] Y. Li, Q. Yuan, D. Guo, C. Lou, X. Cui, G. Mei, H. Petek, L. Cao, W. Ji, and M. Feng, 1D electronic flat bands in untwisted moiré superlattices, Adv. Mater. **35**, 2300572 (2023).

[33] T. Kariyado and A. Vishwanath, Flat band in twisted bilayer Bravais lattices, Phys. Rev. Res. **1**, 033076 (2019).

[34] D. M. Kennes, L. Xian, M. Claassen, and A. Rubio, One-dimensional flat bands in twisted bilayer germanium selenide, Nat. Commun. **11**, 1124 (2020).

[35] M. Fujimoto, T. Kawakami, and M. Koshino, Perfect one-dimensional interface states in a twisted stack of three-dimensional topological insulators, Phys. Rev. Res. **4**, 043209 (2022).

[36] L. Li, Y. Yu, G. J. Ye, Q. Ge, X. Ou, H. Wu, D. Feng, X. H. Chen, and Y. Zhang, Black phosphorus field-effect transistors, Nat. Nanotechnol. **9**, 372 (2014).

[37] J. Qiao, X. Kong, Z.-X. Hu, F. Yang, and W. Ji, High-mobility transport anisotropy and linear dichroism in few-layer black phosphorus, Nat. Commun. **5**, 4475 (2014).

[38] J. Jung, A. Raoux, Z. Qiao, and A. H. MacDonald, *Ab initio* theory of moiré superlattice bands in layered two-dimensional materials, Phys. Rev. B **89**, 205414 (2014).

[39] See Supplemental Material at http://link.aps.org/supplemental/10.1103/PhysRevB.108.L201120 for technical details on first-principles calculations and sliding LL models for coupled wires, which includes Refs. [51–55].

[40] P. Kang, W.-T. Zhang, V. Michaud-Rioux, X.-H. Kong, C. Hu, G.-H. Yu, and H. Guo, Moiré impurities in twisted bilayer black phosphorus: Effects on the carrier mobility, Phys. Rev. B **96**, 195406 (2017).

[41] P. Kang, W. Zhang, V. Michaud-Rioux, X. Wang, J. Yun, and H. Guo, Twistronics in tensile strained bilayer black phosphorus, Nanoscale **12**, 12909 (2020).

[42] N. Marzari and D. Vanderbilt, Maximally localized generalized Wannier functions for composite energy bands, Phys. Rev. B **56**, 12847 (1997).

[43] J. von Delft and H. Schoeller, Bosonization for beginners refermionization for experts, Annalen der Physik **510**, 225 (1998).

[44] T. Giamarchi, *Quantum Physics in One Dimension* (Clarendon Press, Oxford, 2003).

[45] F. Sheng, C. Hua, M. Cheng, J. Hu, X. Sun, Q. Tao, H. Lu, Y. Lu, M. Zhong, K. Watanabe *et al.*, Rashba valleys and quantum Hall states in few-layer black arsenic, Nature (London) **593**, 56 (2021).

[46] R. Mukhopadhyay, C. L. Kane, and T. C. Lubensky, Crossed sliding Luttinger liquid phase, Phys. Rev. B **63**, 081103(R) (2001).

[47] C. L. Kane, R. Mukhopadhyay, and T. C. Lubensky, Fractional quantum Hall effect in an array of quantum wires, Phys. Rev. Lett. **88**, 036401 (2002).

[48] J. C. Y. Teo and C. L. Kane, From Luttinger liquid to non-Abelian quantum Hall states, Phys. Rev. B **89**, 085101 (2014).

[49] T. Neupert, C. Chamon, C. Mudry, and R. Thomale, Wire deconstructionism of two-dimensional topological phases, Phys. Rev. B **90**, 205101 (2014).

[50] P. M. Tam and C. L. Kane, Nondiagonal anisotropic quantum Hall states, Phys. Rev. B **103**, 035142 (2021).

[51] G. Kresse and J. Furthmüller, Efficient iterative schemes for *ab initio* total-energy calculations using a plane-wave basis set, Phys. Rev. B **54**, 11169 (1996).

[52] P. E. Blöchl, Projector augmented-wave method, Phys. Rev. B **50**, 17953 (1994).

[53] J. P. Perdew, K. Burke, and M. Ernzerhof, Generalized gradient approximation made simple, Phys. Rev. Lett. **77**, 3865 (1996).

[54] S. Grimme, J. Antony, S. Ehrlich, and H. Krieg, A consistent and accurate *ab initio* parametrization of density functional dispersion correction (DFT-D) for the 94 elements H-Pu, J. Chem. Phys. **132**, 154104 (2010).

[55] S. Naik, M. H. Naik, I. Maity, and M. Jain, Twister: Construction and structural relaxation of commensurate moiré superlattices, Comput. Phys. Commun. **271**, 108184 (2022).